Journal of Catalysis **182,** 208–218 (1999)
Article ID jcat.1998.2330, available online at http://www.idealibrary.com on IDEAL®

Variable-Temperature Electron Paramagnetic Resonance Studies of Copper-Exchanged Zeolites

Patrick J. Carl and Sarah C. Larsen[1]

Department of Chemistry, University of Iowa, Iowa City, Iowa 52242

Received July 17, 1998; revised November 6, 1998; accepted November 13, 1998

Copper-exchanged zeolites, Beta and ZSM-5, were studied using variable-temperature electron paramagnetic resonance (EPR) spectroscopy to probe changes in the local environment of the Cu^{2+} centers when samples were dehydrated and heated in flowing helium or under reagent flow. Hydrated samples of Cu-ZSM-5 and Cu-Beta exhibited EPR spectra consistent with EPR signals previously assigned to Cu^{2+} in distorted octahedral coordination. EPR spectra of dehydrated Cu-Beta and Cu-ZSM-5 showed the presence of coordination environments that were similar to EPR signals previously assigned to Cu^{2+} in distorted square pyramidal and distorted square planar environments. An empirical model is presented that correlates $g_{\|}$ and $A_{\|}$ for a series of copper-exchanged zeolites and model compounds and provides additional insight into the coordination environment of Cu^{2+} in copper-exchanged zeolites. The empirical model links a number of past EPR studies on different copper-exchanged zeolites and provides an explanation for the observed trends in EPR parameters related to the charge at the copper center. The EPR spectra for dehydrated Cu-ZSM-5 and Cu-Beta samples exhibited a temperature dependence. The EPR spectrum of Cu-ZSM-5 and Cu-Beta recorded at 673 K showed an increase in $g_{\|}$ and a decrease in $A_{\|}$ when compared with the EPR spectrum recorded at room temperature. These changes in spectral parameters are attributed to changes in the electronic environment of the Cu^{2+} species through modification of the coordination environment.

I. INTRODUCTION

Copper-exchanged zeolites are active for the direct decomposition of nitrogen oxides, such as NO_x and nitrous oxide (N_2O) (1–6). NO_x contributes to the production of acid rain and ground-level ozone and is produced during high-temperature combustion in automobiles and in stationary sources, such as power plants. Copper-exchanged ZSM-5 is unique in its demonstrated ability to catalyze the *direct* decomposition of NO_x into nitrogen and oxygen (3, 6, 7). Recently, concerns about nitrous oxide (N_2O) emissions have increased since nitrous oxide is a greenhouse gas with an atmospheric lifetime estimated to be 150 years (290 times that of carbon dioxide). Manmade nitrous oxide is emitted during the production of adipic acid, which is used in the synthesis of nylon. Estimates of the impact of N_2O emissions from adipic acid production suggest that it has caused increases in stratospheric ozone destruction and global warming over the last 10 years (8). Cu-ZSM-5 and Cu-Beta are active for the catalytic decomposition of nitrous oxide into nitrogen and oxygen (5). However, the role of copper in the decomposition of NO_x and N_2O remains unclear. Numerous studies have focused on evaluating the catalytic activity of copper-exchanged zeolites (1–6), and the local environment of copper in the zeolites has been probed using spectroscopic techniques such as Fourier transform infrared (FTIR) (9–16), X-ray adsorption near edge structure (XANES) (7, 17), nuclear magnetic resonance (NMR) (18–20) and electron paramagnetic resonance (EPR) (9, 16, 21–30). In this paper, EPR spectroscopy was used to investigate the coordination of Cu^{2+} in Cu-ZSM-5 and Cu-Beta.

The catalytic activity of copper-exchanged zeolites is influenced by the zeolite structure. The framework of ZSM-5 is composed of straight 10-ring, elliptical channels (pore dimension: 5.3×5.6 Å) running along the [010] direction and sinusoidal 10-ring, elliptical channels (pore dimension: 5.1×5.5 Å) along the [100] direction (31). The framework of zeolite Beta is similar in topology to that of ZSM-5, but the pore size is larger. The framework of Beta is composed of straight 12-ring channels (pore dimension: 5.5×5.5 Å) along the [001] direction and sinusoidal 12-ring, elliptical channels (pore dimension: 7.6×6.4 Å) along the ⟨100⟩ direction (32). The catalytic activity for the decomposition of nitrogen oxides is similar in Cu-ZSM-5 and Cu-Beta.

Determining the location and coordination of copper ions in the zeolite is crucial to understanding the role of copper in the decomposition of nitrogen oxides. EPR spectroscopy has been extensively used to probe the structural environment of paramagnetic copper sites in zeolites (9, 21–25, 27–30). Several groups have studied Cu-ZSM-5 and Cu-Beta using EPR and pulsed EPR techniques (22, 25–30). In previous studies, EPR signals from hydrated Cu-ZSM-5

[1] To whom correspondence should be addressed. Fax: (319) 335–1270. E-mail: sarah-larsen@uiowa.edu.

0021-9517/99 $30.00

samples were assigned to copper species with octahedral coordination. Larsen *et al.* reported that Cu^{2+} in Cu-ZSM-5 underwent autoreduction to Cu^{+} when a hydrated sample was heated and progressively dehydrated (25). These EPR results were supported by an XANES study in which Cu^{+} signals were detected in dehydrated Cu-ZSM-5 (7). The remaining EPR signals in dehydrated Cu-ZSM-5 have been assigned to copper species with distorted square pyramidal and distorted square planar coordinations (22, 24). Similar EPR results have been reported by other groups (9, 25). In this paper, EPR spectroscopy was used to compare the electronic environment and coordination of copper in Cu-ZSM-5 and Cu-Beta. EPR studies of Cu-ZSM-5 and Cu-Beta at typical reaction temperatures (~673 K for emission abatement applications) under helium, as well as under reagent flow, are reported. An empirical model correlating $A_{\parallel}$ and $g_{\parallel}$ for a series of copper-exchanged zeolites is developed. This model is based on EPR studies of Cu^{2+} coordination in model compounds and in proteins (33).

II. EXPERIMENTAL

A. Sample Preparation

Copper-exchanged zeolite Beta (NH_4^+-Beta, Zeolyst Inc.) and ZSM-5 (NaZSM-5, Zeolyst Inc.) were prepared using dilute solutions of copper salts. The parent zeolite (5.0 g) was added to an aqueous copper solution [0.05 M copper(II) nitrate for Cu-Beta preparation and 0.005 M copper(II) acetate for Cu-ZSM-5 preparation] and stirred for 24 h at room temperature. The exchanged zeolite samples were then filtered and washed with 1.0 liters of deionized water and dried overnight in an oven at 363 K. Exchanged samples were characterized by X-ray powder diffraction and inductively coupled plasma atomic emission spectroscopy (ICP-AES) for elemental analysis. X-ray powder diffraction patterns were obtained using a Siemans D5000 diffractometer. Diffraction patterns agreed well with standard diffraction patterns for zeolites Beta and ZSM-5. All of the samples were analyzed using ICP-AES (Perkin Elmer Plasma 400) to determine the Si : Al ratios and the copper loading of the samples. The elemental analysis results are reported in Table 1. Fresh or air-exposed samples are referred to as *hydrated*. The standard sample pretreatment consisted of heating the sample to 673–773 K for 1–2 h in flowing helium. These samples are referred to as *dehydrated*.

TABLE 1

Elemental Analysis Results

Sample	Si : Al	Cu : Al	Cu (wt%)
Cu-Beta	17.8	0.324	1.60
Cu-ZSM-5	15.8	0.203	1.20

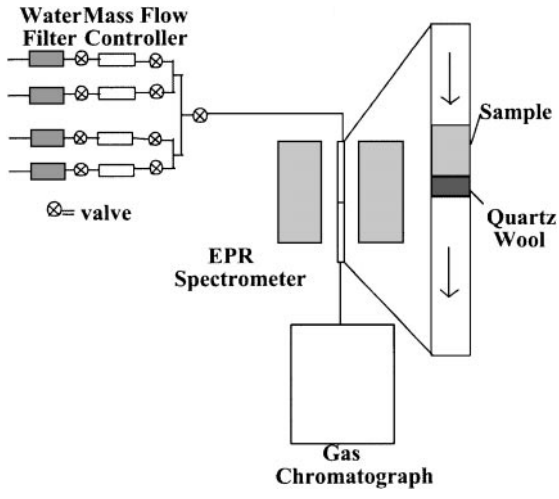

FIG. 1. Schematic of *in situ* EPR apparatus used in this study.

B. Experimental Apparatus

The experimental apparatus is shown in Fig. 1. The system was configured so that *in situ* EPR experiments could be coupled with catalytic activity measurements. The system consists of a Bruker EMX61 EPR spectrometer, a gas flow control system, and a Varian 3400CX gas chromatograph equipped with a thermal conductivity detector (TCD), a flame ionization detector (FID), and a gas sampling valve. The copper-exchanged zeolite sample was placed in an EPR-grade quartz flow tube (i.d. = 1.5 mm) and was held in place by a quartz wool plug. Tylan FC-260 mass flow controllers were used to control the flow of reactant (N_2O in helium) and pretreatment (helium) gases through the flow cell. Hydro-Purge water filters (Alltech) were used to remove water from gases. Product gases were analyzed by injection of a gas sample (0.25 ml) onto a 10-ft, 5-Å molecular sieve column heated to 308 K with a TCD heated to 473 K. The detector was calibrated with 1.01% Nitrogen Primary Standard (Air Products).

For *in situ* EPR experiments, sample pretreatment involved heating approximately 20 mg of the sample under flowing helium (100 cc min^{-1}) to various temperatures in the range 373–673 K and holding at the desired temperature for 30 min. Static adsorption experiments were done on a vacuum rack in EPR sample tubes. For catalytic activity measurements, the sample pretreatment involved heating approximately 40 mg of the sample in 100 cc min^{-1} of helium at 473 K for 1 h followed by heating at 773 K for 1 h. Helium UPC (99.999%, Air Products), Nitrous Oxide Primary Standard (1.00% balanced with helium, Air Products), and Nitrous Oxide Primary Standard (3.99% balanced with helium, Matheson) were used in these studies.

Continuous-wave (CW) EPR spectra were acquired using a Bruker EMX61 equipped with a PC for spectrometer control and data acquisition. A Bruker ER4111 Variable

Temperature Unit with a temperature range of 110–673 K was used to heat and cool the sample. Typical EPR spectral parameters were X-band frequency = 9.43 GHz, modulation amplitude = 10.0 G, and modulation frequency = 100.0 kHz. The magnetic field and microwave frequency were measured using a Hall probe and a frequency counter, respectively.

C. Spectral Simulations

Experimental EPR spectra were fit using second-order perturbation equations (34) for axial A and g combined with a simplex least-squares fitting routine (35). Fit parameters included $A_{\parallel}$, $g_{\parallel}$, $A_{\perp}$, $g_{\perp}$, and Lorenzian and Gaussian broadening factors. Since dehydrated Cu-ZSM-5 samples contain two resolved copper sites, the fitting program was modified to include a set of adjustable parameters for each of the two resolved copper sites and another adjustable parameter representing the relative concentration of each site.

III. RESULTS

Room-temperature EPR spectra of Cu-ZSM-5 after various stages of pretreatment are presented in Fig. 2. The sample was heated to each indicated temperature (373, 473, 573, and 673 K) for 30 min in flowing helium and then cooled to room temperature for EPR data acquisition. The room-temperature EPR spectrum of hydrated Cu-ZSM-5 (Fig. 2A) is broad and structureless, indicating motional broadening as reported previously (22, 25, 36). Resolved, low-field features appeared in the EPR spectrum when the motional effects were reduced by cooling the sample to 120 K. Pretreating the sample at 473, 573, and 673 K in flowing helium resulted in a progressive narrowing of the spectral features consistent with decreasing mobility of the copper ions. Three distinct copper species were identified in the EPR spectrum acquired after pretreatment of Cu-ZSM-5 at 673 K (Fig. 2E). Due to spectral overlap and broadening, we were able to obtain EPR parameters through spectral simulation for only two of the three copper sites. There are two isotopes of copper, ^{63}Cu and ^{65}Cu (both $I = 3/2$), with natural abundances of 69 and 31%, respectively. Spectral simulations indicated that the only resolved feature due to ^{65}Cu is a shoulder on the lowest-field parallel edge of the EPR spectrum of dehydrated Cu-ZSM-5 (and Cu-Beta). No changes in the EPR spectrum were observed after dehydration for longer periods at this temperature or at increased temperatures. As previously observed, the integrated EPR signal intensity of hydrated CuZSM-5 was approximately 2.8 times larger than the integrated EPR signal intensity of CuZSM-5 after standard pretreatment in helium at 673 K (25). This change in intensity was reversible; the full signal intensity was regained when the sample was rehydrated. Comparison of EPR spectra of dehydrated Cu-ZSM-5 taken at room temperature and at 673 K are presented in Fig. 3. The features in the low-field region of the EPR spectrum progressively shift when the sample is heated from room temperature to 673 K. The observed changes in the EPR signal were reversible.

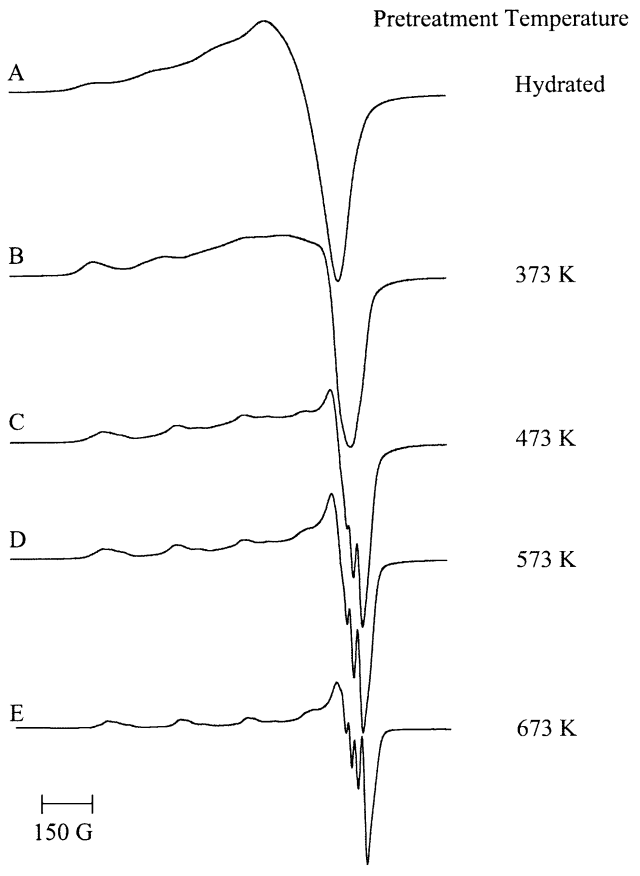

FIG. 2. EPR spectra of Cu-ZSM-5 recorded after pretreatment in helium at the indicated temperatures. Spectra were recorded at room temperature after sequential heating for 30 min at (A) 298 K, (B) 373 K, (C) 473 K, (D) 573 K, and (E) 673 K.

The EPR spectra for the pretreatment of Cu-Beta in helium are presented in Fig. 4. Analogous to Cu-ZSM-5, pretreatment of Cu-Beta was performed by sequentially heating the sample to 373, 473, 573, and 673 K, holding for 30 min at each temperature, and cooling to room temperature for EPR data acquisition. Not shown are spectra obtained after pretreatment at 373 and 573 K, which were similar to spectra obtained after pretreatment at 473 and 673 K, respectively. The EPR spectrum of hydrated Cu-Beta is broad and featureless, consistent with motional broadening. A more resolved spectrum was obtained by cooling the sample to 120 K. After heating to 473 K and above, the low-field features of the EPR spectrum were resolved. The integrated EPR signal intensity of hydrated Cu-Beta was approximately 4.0 times larger than the integrated EPR signal intensity of Cu-Beta after standard pretreatment in

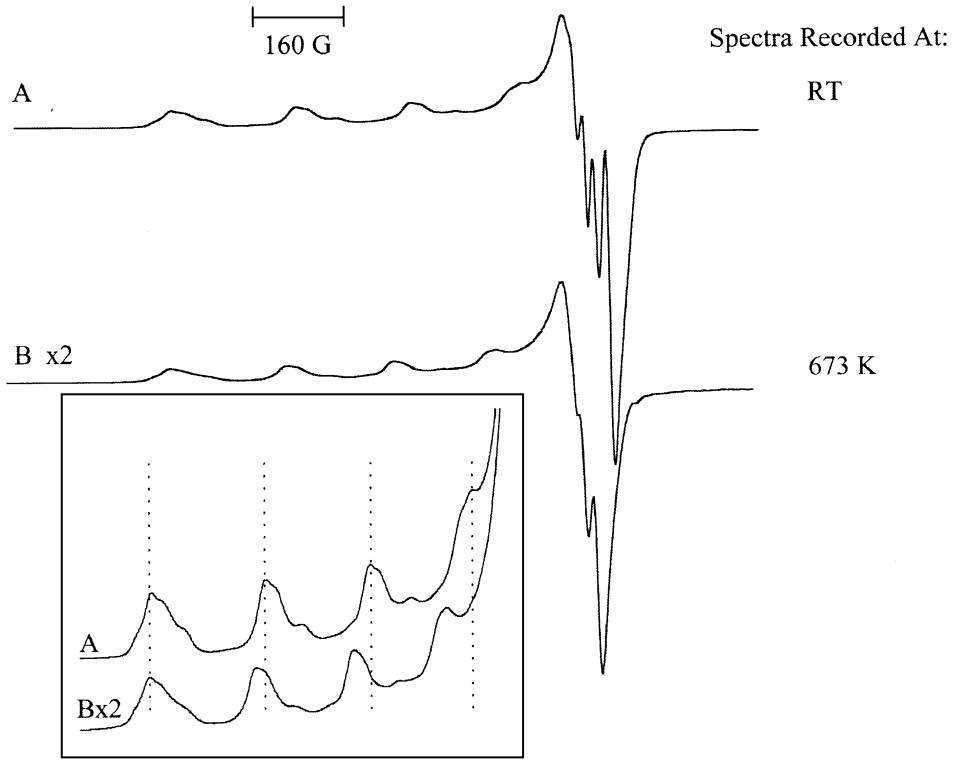

FIG. 3. EPR spectra of dehydrated Cu-ZSM-5 recorded at (A) room temperature and (B) 673 K. Inset: Magnification of low-field region of (A) and (B).

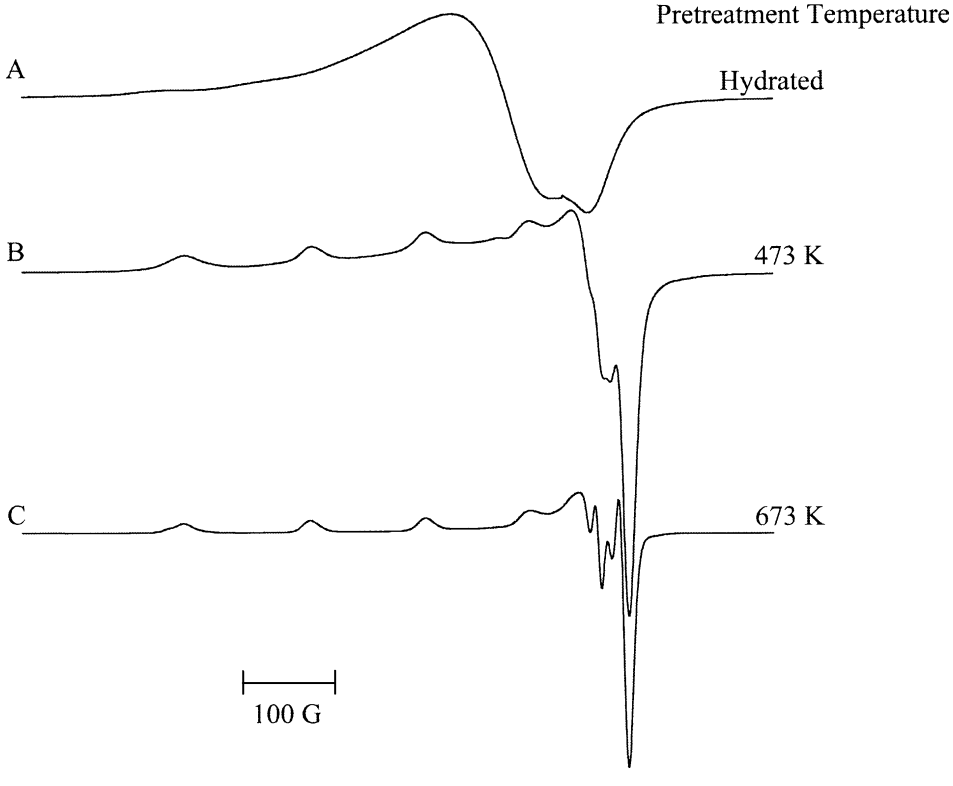

FIG. 4. EPR spectra of Cu-Beta recorded after pretreatment in helium at the indicated temperatures. Spectra were recorded at room temperature after sequential heating for 30 min at (A) 298 K, (B) 473 K, and (C) 673 K.

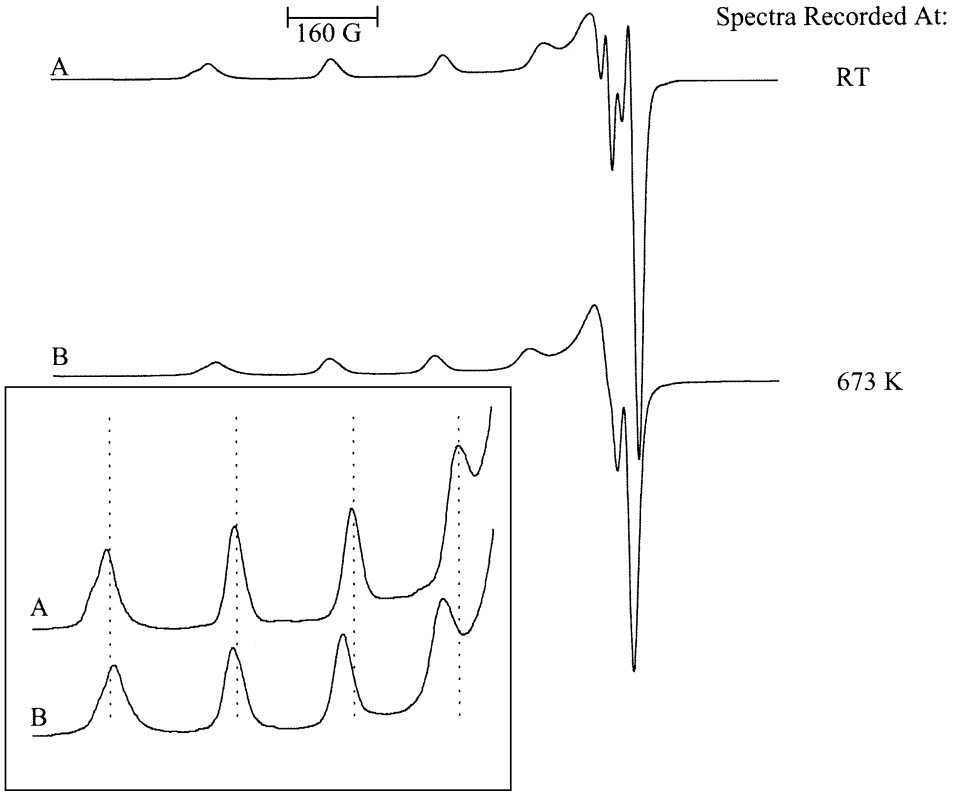

FIG. 5. EPR spectra of dehydrated Cu-Beta recorded at (A) room temperature and (B) 673 K. Inset: Magnification of low-field region of (A) and (B).

helium at 673 K. Just as in the case of Cu-ZSM-5, the change in EPR signal intensity was reversible and the original signal intensity could be regained by rehydration of the sample.

Comparison of EPR spectra of dehydrated Cu-Beta taken at room temperature and at 673 K are presented in Fig. 5. A change in the EPR spectrum was observed as the temperature was increased to 673 K, as was observed in the EPR spectra of Cu-ZSM-5. The low-field features of the spectrum shift as the temperature is increased, indicating a change in the EPR parameters. This change in the EPR spectrum was gradual and reversible. EPR spectra of dehydrated Cu-Beta before and after exposure to xenon are shown in Fig. 6. Dehydration of Cu-Beta (EPR spectrum shown in Fig. 6A) was completed by heating the sample under vacuum, rather than in a helium flow as for the previous Cu-Beta sample (Fig. 5A). The difference in sample preparation may account for the differences in the observed EPR spectrum. The spectral features changed after the addition of ~400 Torr of xenon gas.

The EPR spectra obtained in this study were fit to obtain $g_\parallel$ and $g_\perp$ values and the hyperfine coupling constants, $A_\parallel$ and $A_\perp$ (Tables 2 and 3). The fitting procedure was relatively insensitive to g and A values in the perpendicular region of the EPR spectrum due to lack of resolution in the experimental spectra. The error in EPR parameters obtained from the fitting procedure was estimated to be ± 0.001 for $g_\parallel$ and ± 5 MHz for $A_\parallel$. Errors in $g_\perp$ and $A_\perp$ were estimated to be larger, ± 0.005 for $g_\perp$ and ± 10 MHz for $A_\perp$, due to the insensitivity of the fitting procedure in this region of the EPR spectrum. Representative EPR spectra of dehydrated CuZSM-5 and dehydrated Cu-Beta and their respective spectral simulations obtained using the least-squares fitted parameters in Table 3 are given in Figs. 7 and 8.

EPR spectra (not shown) of Cu-Beta and Cu-ZSM-5 were also recorded in the presence of flowing N_2O (0.13% in

TABLE 2

Fitted EPR Parameters for Hydrated Cu-Exchanged Zeolites[a,b]

Sample	$g_\parallel$	$A_\parallel$ (MHz)	$g_\perp$	$A_\perp$ (MHz)	Reference
Cu-ZSM-5 (120 K)	2.385	449	2.084	0	This work
Cu-Beta (120 K)	2.398	460	2.083	0	This work
Cu-ZSM-5 (77 K)	2.379	456	2.076	—	(22)
Cu-Beta	2.379	350	2.08	—	(30)
Cu-ferrierite	2.397	450	2.076	—	(21)

[a] The temperature in parentheses indicates the temperature at which the EPR spectrum was recorded.

[b] Estimated errors: $g_\parallel = \pm 0.001$, $A_\parallel = \pm 5$ MHz; $g_\perp = \pm 0.005$, $A_\perp = \pm 10$ MHz.

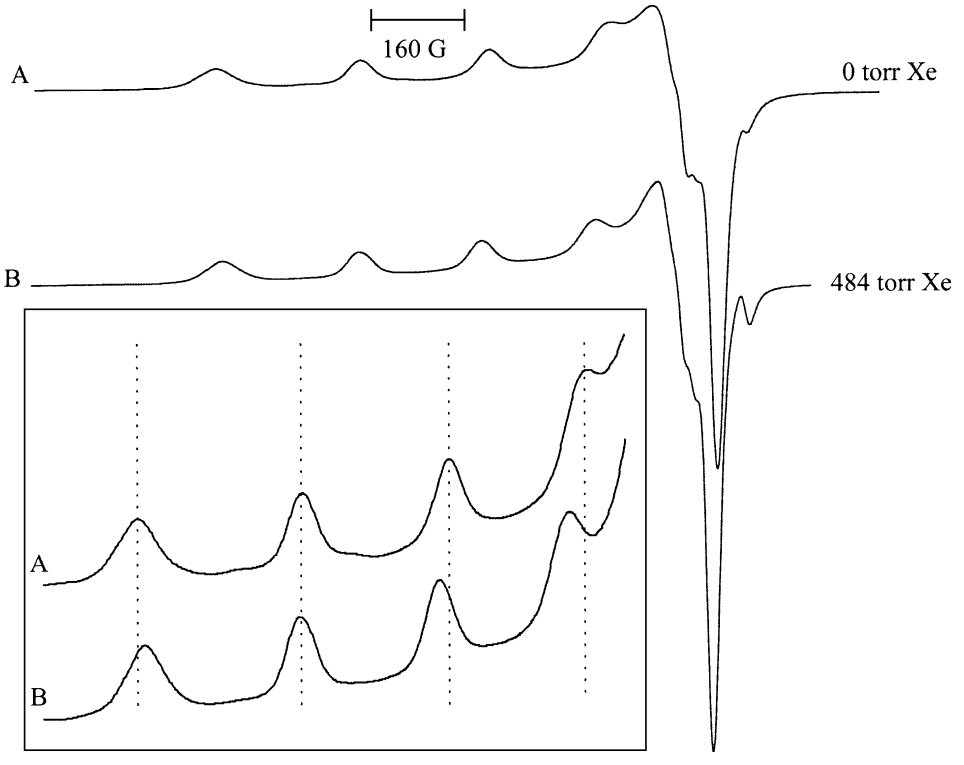

FIG. 6. EPR spectra of dehydrated Cu-Beta (A) before and (B) after adsorption of xenon. Cu-Beta was dehydrated by heating to 673 K under vacuum. EPR spectra were recorded at room temperature. Inset: Magnification of low-field region of (A) and (B).

He) at room temperature and 673 K. No changes in the EPR spectra were observed when the catalysts were exposed to N_2O at either of these temperatures. Under these conditions, the conversion of N_2O to N_2 was 10% for Cu-Beta and 5% for Cu-ZSM-5. However, *ex situ* experiments that measured the conversion of N_2O to N_2 on these catalysts

TABLE 3

Fitted EPR Parameters for Dehydrated Cu-Exchanged Zeolites[a–c]

Sample	$g_\parallel$	$A_\parallel$ (MHz)	$g_\perp$	$A_\perp$ (MHz)	Reference
Cu-ZSM-5 (RT)[d]					
1	2.306	520	2.055	9	This work
2	2.270	549	2.073	10	This work
Cu-ZSM-5 (673 K)	2.324	474	2.067	24	This work
Cu-Beta (RT)	2.314	520	2.070	33	This work
Cu-Beta (673 K)	2.320	480	2.067	9	This work
Cu-Beta (xenon)	2.318	508	2.068	25	This work
Cu-ZSM-5 (77 K)	2.310	516	2.052	—	(22)
Cu-Beta	2.318	516	2.05	90	(30)
Cu-ferrierite	2.330	525	2.069	54	(21)

[a] The temperature in parentheses indicates the temperature at which the EPR spectrum was recorded. RT, room temperature.

[b] Dehydrated refers to samples that have been pretreated in helium at 673 K for at least 1 h.

[c] Estimated errors: $g_\parallel = \pm 0.001$, $A_\parallel = \pm 5$ MHz; $g_\perp = \pm 0.005$, $A_\perp = \pm 10$ MHz.

[d] Relative amount of species 1 to that of species 2 = 2.3.

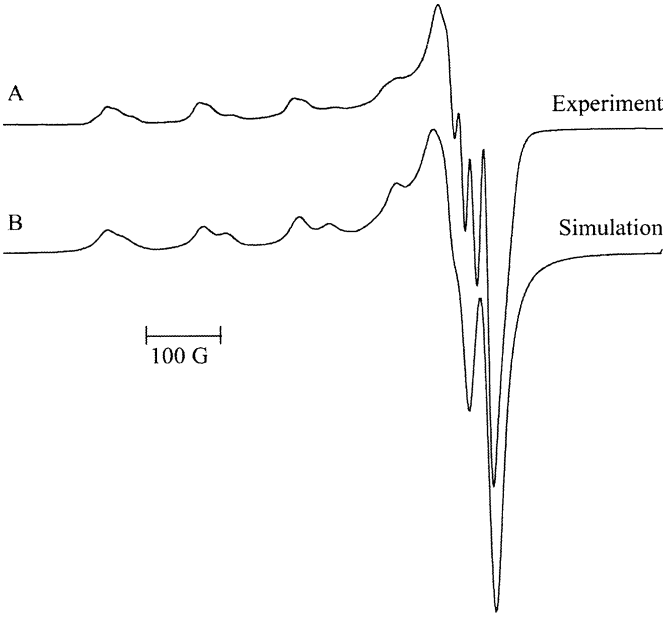

FIG. 7. (A) Experimental and (B) simulated EPR spectra of dehydrated Cu-ZSM-5. The experimental EPR spectrum was recorded at room temperature.

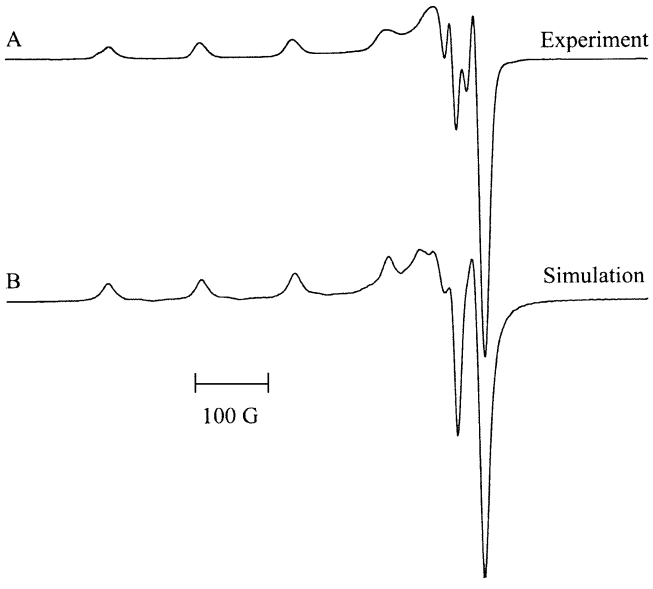

FIG. 8. (A) Experimental and (B) simulated EPR spectra of dehydrated Cu-Beta. The experimental EPR spectrum was recorded at room temperature.

at higher temperatures show that the amount of N_2O converted begins to increase at about 673 K.

IV. DISCUSSION

A. *Assignment of Cu^{2+} EPR Spectra*

Structural information about copper sites in zeolites can be obtained from EPR spectra. The hyperfine coupling between the 3*d* unpaired electron and the nuclear spin ($I = 3/2$) of Cu^{2+} results in a fourfold splitting of the EPR line. For an orientationally disordered solid with axial symmetry, *g* anisotropy produces a powder pattern in which the sharp features are referred to as the parallel and perpendicular edges of the spectrum. A typical copper EPR spectrum for an orientationally disordered solid with axial symmetry consists of four resolved low-field features which are referred to as the parallel edges of the spectrum. The perpendicular edges at the low-field end of the powder pattern are generally unresolved for copper-exchanged zeolites due to broadening from site inhomogeneity.

The EPR spectra of hydrated Cu-ZSM-5 and Cu-Beta obtained in this study were similar to those reported previously (22). The room-temperature EPR spectra of hydrated Cu-ZSM-5 and Cu-Beta were broad, indicating motion of the copper complex. At 120 K, the motion of the copper complex was reduced and the hyperfine features were resolved in the EPR spectra of hydrated Cu-ZSM-5 and Cu-Beta. The fitted $g_\parallel$ and $A_\parallel$ values for low-temperature EPR spectra of hydrated Cu-ZSM-5 and Cu-Beta ($g_\parallel = 2.385$ and $A_\parallel = 449$ MHz for Cu-ZSM-5; $g_\parallel = 2.398$ and $A_\parallel = 460$ MHz for Cu-Beta) are in good agreement with those previously assigned to octahedrally coordinated hydrated copper ions in Cu-ZSM-5 ($g_\parallel = 2.379$, $A_\parallel = 456$ MHz) (22) and in other copper-exchanged zeolites (21, 22, 25) (Table 2). Oliva and co-workers observed very different $g_\parallel$ and $A_\parallel$ values ($g_\parallel = 2.379$, $A_\parallel = 350$ MHz) for hydrated Cu-Beta in their EPR study (30). This is surprising to us since the agreement between their data and ours for the dehydrated Cu- Beta is very good.

During the progressive dehydration of Cu-ZSM-5 and Cu-Beta several changes in the EPR spectra were observed. First, the overall intensity of the EPR spectrum decreased by approximately 65–75% when comparing the EPR spectrum of *hydrated* Cu-ZSM-5 (or Cu-Beta) with the EPR spectrum of *dehydrated* Cu-ZSM-5 (or Cu-Beta). This has previously been attributed to the autoreduction of Cu^{2+} (paramagnetic) to Cu^{+} (diamagnetic) for copper-exchanged ZSM-5 (1, 20, 25, 37, 38). The decrease in EPR intensity after dehydration has also been previously observed in EPR spectra of Cu-Beta (30). Kucherov *et al.* claimed that autoreduction does not occur in Cu-ZSM-5, but they examined the temperature dependence of the EPR signal of dehydrated Cu-ZSM-5 rather than the change in signal intensity between a hydrated and a dehydrated sample (39). Second, the parallel features of the EPR spectrum of dehydrated Cu-ZSM-5 and Cu-Beta were resolved at room temperature, suggesting that the Cu^{2+} center is no longer mobile at room temperature and is bound to oxygen in the zeolite lattice. Third, the EPR spectral features changed considerably as the coordination of Cu^{2+} changed when it was dehydrated and bonded to oxygen in the zeolite framework.

The fitted *g* and *A* values for dehydrated Cu-ZSM-5 and Cu-Beta are given in Table 3. Two species, 1 and 2 (relative concentrations 2 : 1), are identified in dehydrated Cu-ZSM-5, but only one major species is observed in dehydrated Cu-Beta. The EPR spectrum of dehydrated Cu-Beta is shown in Fig. 8 along with the spectral simulation obtained using the parameters in Table 3 that were determined from a least-squares fit to the data. The fitted EPR parameters of species 1 in Cu-ZSM-5 ($g_\parallel = 2.306$, $A_\parallel = 520$ MHz) are very similar to those of the copper species present in dehydrated Cu-Beta ($g_\parallel = 2.314$, $A_\parallel = 520$ MHz) and have previously been assigned to Cu^{2+} in a distorted square pyramidal coordination environment (24, 27, 40). Oliva *et al.* observed a copper species in Cu-Beta with similar EPR parameters ($g_\parallel = 2.318$, $A_\parallel = 518$ MHz) (30). The observed increase in $A_\parallel$ and decrease in $g_\parallel$ in the hydrated versus the dehydrated EPR spectrum of Cu-ZSM-5 and Cu-Beta has previously been interpreted as a change in the coordination of the copper center from six-coordinate (octahedral) to five-coordinate (square pyramidal) (24, 27). The fitted EPR parameters for species 2 ($g_\parallel = 2.270$, $A_\parallel = 549$ MHz) in Cu-ZSM-5 correspond to those previously assigned to

Cu^{2+} in a distorted square planar environment (24, 27, 40). The assignment of these EPR signals to Cu^{2+} in distorted square pyramidal and distorted square planar coordination is based on model compound studies and therefore the coordination should be considered a "best estimate" of the coordination of copper in the zeolite. It is likely that in the zeolite, distortions from ideal octahedral, square planar, and square pyramidal coordinations exist.

In a recent study by Attfield *et al.* (21), EPR spectroscopy and synchrotron X-ray powder diffraction were used to investigate Cu-ferrierite, another active catalyst for the decomposition of nitrogen oxides. The ferrierite structure consists of oval, 10-ring channels (pore dimension: 4.2×5.4 Å) that intersect 8-ring channels (pore dimension: 3.5×4.8 Å). Based on Rietvald refinement of the synchrotron X-ray diffraction data, a copper site was identified that is located at the edge of the 8-ring at the intersection of the 8-ring and 10-ring channels. This copper species has two short bonds (2.03 and 2.21 Å) to framework oxygen atoms. One species was observed in the EPR spectrum of dehydrated Cu-ferrierite with parameters of $g_{\|} = 2.330$, $A_{\|} = 525$ MHz, $g_{\perp,yy} = 2.069$, $g_{\perp,xx} = 2.056$ (21). This nonaxial copper EPR signal was attributed to the copper site identified by X-ray diffraction. The authors suggested that the poor coordination of the copper and its location near the channel intersection make the copper more accessible to NO and more susceptible to redox chemistry.

The EPR parameters obtained for the copper species in dehydrated Cu-ZSM-5 (species 1) and dehydrated Cu-Beta in this study exhibit slightly smaller $g_{\|}$ and slightly larger $A_{\|}$ than those for dehydrated Cu-ferrierite reported by Attfield *et al.* The copper EPR signals in the dehydrated zeolites were assigned to two-coordinate (Cu-ferrierite, Attfield *et al.* work) or five-coordinate (Cu-ZSM-5 and Cu-Beta, this work) copper species. In all cases, it can be argued that the accessibility of the copper ions to reactants such as NO and N_2O increases as the coordination number decreases in the dehydrated zeolites.

In the next section, the EPR spectral parameters for copper-exchanged zeolites are discussed in the context of an empirical model developed by Peisach and Blumberg for interpreting the EPR spectra of Cu^{2+} in model compounds and proteins (33).

B. Comparison of EPR Data for Copper-Exchanged Zeolites and Model Compounds

EPR spectroscopy has been used very successfully to probe the ligand environment of Cu^{2+} in proteins (33, 41, 42). Peisach and Blumberg developed empirical correlations between $A_{\|}$ and $g_{\|}$ for a series of Cu^{2+} model compounds with varying ligands and well-defined structures (33). Trends were found that enabled Cu^{2+} EPR parameters to be correlated to the copper ligands and the overall charge of the model complexes in solution. The plots of $g_{\|}$ versus $A_{\|}$ for a series of model compounds with different ligands produced straight lines; the slope and position of the lines were dependent on the identity of the ligands (33). Copper proteins were classified into two groups according to their EPR parameters and the coordinated ligands were identified based on comparisons with the model compound data (33).

To further evaluate our Cu^{2+} EPR data in the context of past EPR work in copper-exchanged zeolites, Cu^{2+} proteins, and model compounds, we made plots correlating $A_{\|}$ and $g_{\|}$ for copper-exchanged zeolites and for square planar model compounds with four oxygen ligands. The filled circles in Fig. 9 represent Peisach and Blumberg's correlation plot for Cu^{2+} model compounds with four oxygen ligands. The bar shows the charge of the model Cu^{2+} complexes. A trend in $A_{\|}$ and $g_{\|}$ was observed as the charge of the model complex was varied from 2+ $[Cu(H_2O)_4^{2+}]$ to 2− $[Cu(OH)_4^{2-}]$. The observed trend corresponded to an increase in $A_{\|}$ and a decrease in $g_{\|}$ with increasing negative charge on the copper center or increasing delocalization of the charge on the copper center. This correlation in $A_{\|}$ and $g_{\|}$ was reproduced in our data for Cu-ZSM-5 and Cu-Beta as indicated by the open symbols in Fig. 9. This is consistent with the assignment of the hydrated copper in Cu-ZSM-5 and Cu-Beta to a distorted octahedral water complex $[Cu(H_2O)_5OH^+]$ with an overall charge of 1+. The Cu^{2+} complexes in dehydrated Cu-ZSM-5 and dehydrated Cu-Beta are not as well defined, in terms of ligands. The common assumption is that Cu^{2+} is bound to oxygen in the zeolite lattice and possibly to OH^-, producing copper complexes with formal charges of less than 2+. The trend in going from octahedral to square planar to square pyramidal not only represents a change in the coordination of

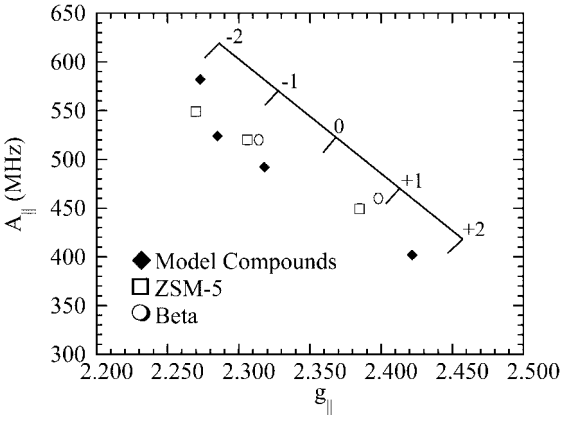

FIG. 9. Plot of $g_{\|}$ versus $A_{\|}$ for copper-exchanged ZSM-5 and Beta (open symbols) from this work and for a series of Cu^{2+} model complexes (filled symbols) from Refs. (45–47). The bar represents the charge of the model complexes ranging from +2 to −2 according to Peisach and Blumberg (33).

Cu^{2+}, but also represents a change in the delocalized charge experienced by the copper center as discussed above.

Figures 7 and 8 show the comparison of the experimental and simulated (from best-fit parameters) EPR spectra for dehydrated Cu-ZSM-5 and Cu-Beta. The broadening of the experimental spectra is not reproduced very well in the simulated spectra (Lorentzian and Gaussian factors) due to the effects of g and A strain. If g and A strain, which is caused by a range of values for g and A due to differences in local environments, is responsible for the observed broadening of the EPR spectra, then the g and A strain should be correlated according to the Peisach–Blumberg correlation plot shown in Fig. 9. Spectral simulations incorporating a correlated g and A strain have been completed and show that correlated g and A strain cause the broadening to increase with magnetic field strength as is experimentally observed. The correlated g and A strain was simulated by assuming that for a given distribution of $g_\parallel$ values, the $A_\parallel$ values were determined from $g_\parallel$ using the best-fit line to the data in Fig. 9.

EPR spectral parameters obtained from our group and from other groups for copper-exchanged zeolites are presented in Fig. 10. Only EPR parameters obtained through spectral simulation were plotted in Fig. 10 and error bars were graphed when provided. Table 4 gives a complete list of the literature data plotted in Figs. 9 and 10. The EPR data for the copper-exchanged zeolites form two groups as indicated by the ellipses in Fig. 10. Group 1 includes copper-exchanged Beta, ZSM-5, and ferrierite and these data span the range of the Cu^{2+} oxygen model complexes studied by Peisach and Blumberg (33). Group 2 includes copper-exchanged mordenite, Y, and X, and the EPR parameters for these zeolites are found in the lower ellipse. [The data point for hydrated Cu-Beta from the work of Oliva is in the region defined as group 2 and is the one exception to this grouping of copper-exchanged zeolites (30).] The $A_\parallel$ values for group 2 zeolites are approximately 20% smaller than the $A_\parallel$ values for group 1 zeolites for a given $g_\parallel$ value. The trend of increasing $A_\parallel$ and decreasing $g_\parallel$ with overall charge of the copper complex is observed within each group of copper-exchanged zeolites. The hydrated copper-exchanged zeolites exhibit $A_\parallel$ and $g_\parallel$ values represented by the lower right-hand portion of each ellipse. The dehydrated copper-exchanged zeolites are represented by data in the center and upper left-hand regions of each ellipse corresponding to complexes with an overall charge of less than 2+.

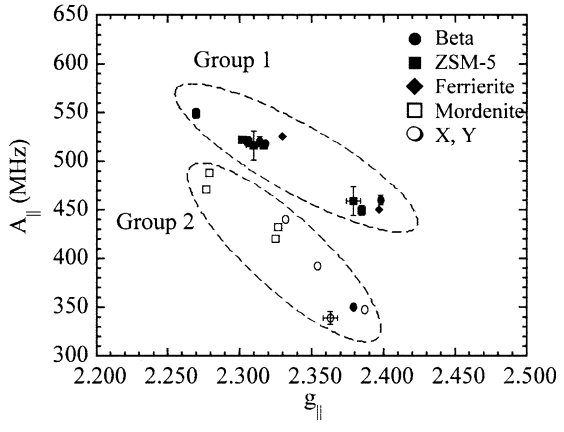

FIG. 10. Plot of $g_\parallel$ versus $A_\parallel$ for copper-exchanged zeolites compiled from the literature (Table 4) and from this work. The filled symbols are labeled as group 1 and represent EPR data compiled from the literature and from this work for copper-exchanged ZSM-5, Beta, and ferrierite. The open symbols are labeled as group 2 and represent EPR data compiled from the literature for copper-exchanged mordenite, X, and Y.

TABLE 4

Literature EPR Parameters for Cu-Exchanged Zeolites

Sample	$g_\parallel$	$A_\parallel$ (MHz)	Reference
Cu-ferrierite	2.397	450	(21)
	2.330	525	(21)
Cu-ZSM-5	2.379	459	(22)
	2.317	516	(43)
	2.310	516	(22)
	2.302	522	(43)
Cu-Beta	2.379	350	(30)
	2.318	518	(30)
Cu-mordenite	2.327	432	(44)
	2.325	420	(30)
	2.279	488	(44)
	2.277	471	(27)
Cu-X,Y	2.387	348	(27)
	2.363	339	(18)
	2.354	392	(27)
	2.332	440	(27)
AQ $[Cu(H_2O)_6^{2+}]$	2.422	402	(45)
OX $[Cu(ox)_2^{2-}]$	2.318	492	(45)
AQ3 $[Cu(OH)_4^{2-}]$	2.273	582	(46)
ACA $[Cu(acac)_2]$	2.285	524	(47)

The empirical correlation between $A_\parallel$ and $g_\parallel$ suggests that the charge at the copper center may be the most important factor in determining the relative sizes of $A_\parallel$ and $g_\parallel$ rather than the coordination of the copper complex. This explanation is compatible with previous interpretations of EPR data that assign specific EPR signals in copper-exchanged zeolites to distorted octahedral, distorted square planar, and distorted square pyramidal environments. This comparison also shows that the copper sites in copper-exchanged zeolites within group 1 and within group 2 exhibit similar trends in $A_\parallel$ and $g_\parallel$ with charge of the copper complex. The empirical model presented here links a number of past EPR studies on different copper-exchanged zeolites and provides an alternative explanation for the observed trends in EPR parameters.

The similarities in the copper environments in different zeolites, particularly in Cu-exchanged ZSM-5, Beta, and

ferrierite, and the correspondence to Cu^{2+} model compounds with oxygen ligands are remarkable. However, it should be recognized that the electronic environment of copper in frozen solutions of model compounds and in zeolites may be very different, and therefore, it is possible that this simple correlation does not present a complete picture of the factors governing the copper electronic environment in zeolites. For example, the chosen model compounds had well-defined structures that did not change as the ligand was varied. In the zeolite, the ligand changed from water to oxygen when the copper-exchanged zeolite was dehydrated, and the geometry around the copper center also changed. In addition, the geometries of copper complexes found in zeolites are expected to be distorted from ideal geometries. It should also be pointed out that the combination of charge and coordination of the copper complex are interrelated and both factors may potentially affect the local density of charge at the copper site and, therefore, the observed EPR spectrum.

The systematically lower $A_\parallel$ values observed for group 2 zeolites (copper-exchanged mordenite, Y, and X) in the correlation plot could be due to the lower Si : Al ratio. The zeolites constituting group 2 in Fig. 10 all have Si : Al ratios below 10, while the zeolites in group 1 have Si : Al ratios greater than 10. Work is in progress to compare the Cu^{2+} EPR signals from a series of mordenite and Y zeolites with varying Si : Al ratios to test this hypothesis. Peisach and Blumberg suggest that small deviations from square planar geometry may cause a decrease in $A_\parallel$ and, for large deviations, a decrease in $g_\parallel$ as well (33). This suggests that a distortion of the square planar geometry in the group 2 zeolites could cause the observed decrease in $A_\parallel$. Another alternative explanation involving the electronic properties of oxygen in different zeolites should also be considered. Schoonhedyt *et al*. have observed that the *softness* of oxygen in copper-exchanged zeolites as defined by the energy of the ligand-to-metal charge transfer transition (LMCT) can be correlated with $g_\parallel$ and $A_\parallel$ (27). They found that $g_\parallel$ decreases and $A_\parallel$ increases with increasing softness of the oxygens in the first coordination sphere (27). The softness of copper-exchanged zeolites exhibits the trend ZSM-5 > mordenite > X, Y, suggesting that group 1 zeolites have oxygen atoms with greater oxygen softness than group 2 zeolites.

C. Temperature Dependence of the Copper EPR Signals

A comparison of the EPR spectra for Cu-ZSM-5 and Cu-Beta at room temperature and at 673 K shows changes in EPR spectra as a function of temperature. Table 3 lists the fitted EPR parameters obtained from a least-squares fit to the EPR spectra shown in Figs. 3 and 5. The EPR parameters for species 1 in dehydrated Cu-ZSM-5 changed with temperature as follows: $g_\parallel$ increased from 2.306 at room temperature to 2.324 at 673 K while $A_\parallel$ decreased from 520 MHz at room temperature to 474 MHz at 673 K. EPR spectra of dehydrated Cu-Beta in the temperature range 373–673 K showed a similar effect. In Cu-Beta, $g_\parallel$ increased from 2.314 at room temperature to 2.320 at 673 K, while $A_\parallel$ decreased from 520 MHz at room temperature to 480 MHz at 673 K. The EPR spectrum of dehydrated Cu-Beta at 673 K is shown in Fig. 8 along with the spectral simulation obtained using the parameters in Table 3 that were determined from a least-squares fit to the data. This change in the EPR spectrum of Cu-ZSM-5 and Cu-Beta suggests a temperature-dependent change in the average electronic environment of the copper species possibly corresponding to a distortion or change in the average symmetry of Cu^{2+} in ZSM-5 and Beta. The observed change in EPR parameters is too small to suggest a large change in charge or coordination of the Cu^{2+}.

Adsorption of xenon into Cu-Beta also caused a change in the Cu^{2+} EPR spectrum. The EPR parameters (Table 3) derived from a least-squares fit of the EPR spectra in Fig. 6 show a decrease in $A_\parallel$ from 520 to 508 MHz when xenon was adsorbed on Cu-Beta. The observed change in EPR spectrum when xenon was adsorbed was smaller in magnitude, but in the same direction as the shift observed in Cu-Beta recorded at 673 K. Kucherov and Slinkin observed a similar effect on adsorption of xenon on Cu-HZSM-5 and attributed the change in EPR spectrum to a displacement of pentacoordinated Cu^{2+} due to dispersion forces (36).

The observed changes in the EPR spectrum with temperature are particularly important from the perspective of catalysis, since the onset of catalytic activity for nitrogen oxide decomposition occurs at about 673 K. No changes in the EPR spectra were observed when Cu-Beta was exposed to N_2O at 673 K or at room temperature, suggesting that on the time scale of the EPR experiment, no change in the average oxidation state or coordination of the copper center occurred. However, the EPR results reported here do suggest that the copper environments in Cu-ZSM-5 and Cu-Beta change at high temperature due to a symmetry change or distortion of the Cu^{2+} coordination environment. Perhaps this change in local environment of the copper facilitates reaction with NO or N_2O by increasing the accessibility of reactant molecules to Cu^{2+}.

V. CONCLUSIONS

Copper-exchanged zeolites Beta and ZSM-5 were studied using variable-temperature electron paramagnetic resonance spectroscopy. The EPR spectra of hydrated Cu-ZSM-5 and hydrated Cu-Beta corresponded very well with EPR spectra previously assigned to distorted octahedrally coordinated copper species in copper-exchanged zeolite. EPR spectra of dehydrated Cu-ZSM-5 and dehydrated Cu-Beta exhibited spectral features consistent with EPR signals previously assigned to Cu^{2+} in distorted square planar

and distorted square pyramidal coordination environments. The observed decrease in coordination may increase the accessibility of copper to reactant molecules.

An empirical model was presented that correlates $g_{\|}$ and $A_{\|}$ for a series of copper-exchanged zeolites and model complexes and provides additional insight into the coordination environment of Cu^{2+} in copper-exchanged zeolites. The correlation between $g_{\|}$ and $A_{\|}$ for oxygen-ligated Cu^{2+} model complexes and copper-exchanged zeolites was remarkable. The results suggested that the charge at the copper center may be the most important factor governing the observed trend in $g_{\|}$ and $A_{\|}$.

The EPR spectra of dehydrated Cu-ZSM-5 and dehydrated Cu-Beta recorded at 673 K showed an increase in $g_{\|}$ and a decrease in $A_{\|}$ when compared with the EPR spectrum recorded at room temperature. These changes in spectral parameters are attributed to changes in the electronic environment of the copper(II) species through modification of the coordination environment.

ACKNOWLEDGMENTS

Acknowledgment is made to the University of Iowa for support of this work. The authors also thank Professor John Wiencek for use of his ICP/AES instrument and Professor Gary Gerfen for helpful discussions.

REFERENCES

1. Iwamoto, M., Yahiro, H., Tanda, K., Mizuno, N., Mine, Y., and Kagawa, S., *J. Phys. Chem.* **95**, 3727 (1991).
2. Iwamoto, M., Furukawa, H., and Kagawa, S., "Catalytic Decomposition of Nitric Monoxide over Copper Ion-Exchanged Zeolites." Elsevier, New York, 1986.
3. Li, Y., and Armor, J. N., *Appl. Catal. B Environ.* **3**, L1 (1993).
4. Shelef, M., *Chem. Rev.* **95**, 209 (1995).
5. Li, Y., and Armor, J. N., *Appl. Catal. B Environ.* **1**, L21 (1992).
6. Li, Y., and Hall, W. K., *J. Phys. Chem.* **64**, 6145 (1990).
7. Grunert, W., Hayes, N. W., Joyner, R. W., Shpiro, E. S., Siddiqui, M. R. H., and Baeva, G. N., *J. Phys. Chem.* **98**, 10832 (1994).
8. Reimer, R. A., Slaten, C. S., Seapan, M., Lower, M. W., and Tomlinson, P. E., *Environ. Prog.* **13**, 134 (1994).
9. Dedecek, J., Sobalik, Z., Tvaruzkova, Z., Kaucky, D., and Wichterlova, B., *J. Phys. Chem.* **99**, 16327 (1995).
10. Wichterlova, B., Dedecek, J., Sobalik, Z., Vondrova, A., and Klier, K., *J. Catal.* **169**, 194 (1997).
11. Cheung, T., Bhargava, S. K., Hobday, M., and Foger, K., *J. Catal.* **158**, 301 (1996).
12. Szanyi, J., and Paffett, M. T., *J. Catal.* **164**, 232 (1996).
13. Aylor, A., Larsen, S. C., Reimer, J. A., and Bell, A. T., *J. Catal.* **157**, 592 (1995).
14. Valyon, J., and Hall, W. K., *J. Phys. Chem.* **97**, 7054 (1993).
15. Sarkany, J., d'Itri, J., and Sachtler, W. M. H., *Catal. Lett.* **16**, 241 (1992).
16. Giamello, E., Murphy, D., Magnacca, G., Morterra, C., Shioya, Y., Nomura, T., and Anpo, M., *J. Catal.* **136**, 510 (1992).
17. Liu, D.-J., and Robota, H. J., *Catal. Lett.* **21**, 291 (1993).
18. Liu, S.-B., Lin, T.-S., Yang, T.-C., Chen, T.-H., Hong, E.-C., and Ryoo, R., *J. Phys. Chem.* **99**, 8277 (1995).
19. Gedeon, A., Bonardet, J. L., and Fraissard, J., *J. Phys. Chem.* **97**, 4254 (1993).
20. Hu, S., Reimer, J. A., and Bell, A. T., *J. Phys. Chem. B* **101**, 1869 (1997).
21. Attfield, M. P., Weigel, S. J., and Cheetham, A. K., *J. Catal.* **170**, 277 (1997).
22. Anderson, M. W., and Kevan, L., *J. Phys. Chem.* **91**, 4174 (1987).
23. Kucherov, A. V., Kucherova, T. N., and Slinkin, A. A., *Catal. Lett.* **10**, 289 (1991).
24. Kucherov, A. V., Slinkin, A. A., Kondrat'ev, D. A., Bondarenko, T. N., Rubinstein, A. M., and Minachev, K. M., *Zeolites* **5**, 320 (1985).
25. Larsen, S. C., Aylor, A., Bell, A. T., and Reimer, J. A., *J. Phys. Chem.* **98**, 11533 (1994).
26. Sass, C. E., and Kevan, L., *J. Phys. Chem.* **93**, 7856 (1989).
27. Schoonheydt, R. A., *Catal. Rev. Sci. Eng.* **35**, 129 (1993).
28. Kucherov, A. V., Gerlock, J. L., Jen, H.-W., and Shelef, M., *J. Catal.* **152**, 63 (1995).
29. Kucherov, A. V., Hubbard, C. P., and Shelef, M., *J. Catal.* **157**, 603 (1995).
30. Oliva, C., Selli, E., Ponti, A., Correale, L., Solinas, V., Rombi, E., Monaci, R., and Forni, L., *J. Chem. Soc. Faraday Trans.* **93**, 2603 (1997).
31. Kokotailo, G. T., Lawton, S. L., Olson, D. H., and Meier, W. M., *Nature* **272**, 437 (1978).
32. Higgins, J. B., LaPierre, R. B., Schlenker, J. L., Rohrman, A. C., Wood, J. D., Kerr, G. T., and Rohrbaugh, W. J., *Zeolites* **8**, 446 (1988).
33. Peisach, J., and Blumberg, W. E., *Arch. Biochem. Biophys.* **165**, 691 (1974).
34. Chasteen, N. D., *in* "Vanadyl(IV) EPR Spin Probes: Inorganic and Biochemical Aspects" (L. J. Berliner and J. Reuben, Eds.), Vol. 3, p. 53. Plenum, New York, 1981.
35. Press, W. H., Teukolsky, S. A., Vetterling, W. T., and Flannery, B. P., "Numerical Recipes in C," 2nd ed. Cambridge Univ. Press, New York, 1992.
36. Kucherov, A. V., and Slinkin, A. A., *J. Phys. Chem.* **93**, 864 (1989).
37. Jang, H.-J., Hall, W. K., and d'Itri, J. L., *J. Phys. Chem.* **100**, 9416 (1996).
38. Li, Y., and Hall, W. K., *J. Catal.* **129**, 202 (1991).
39. Kucherov, A. V., Gerlock, J. L., Jen, H.-W., and Shelef, M., *J. Phys. Chem.* **98**, 4892 (1994).
40. Smith, D. W., *J. Chem. Soc. (A)*, 3108 (1970).
41. Vanngard, T., *in* "Biological Applications of Electron Spin Resonance" (H. M. Swartz, J. R. Bolton, and D. C. Borg, Eds.), p. 411. Wiley–Interscience, New York, 1972.
42. Boas, J. F., Pilbrow, J. R., and Smith, T. D., *in* "ESR of Copper in Biological Systems" (L. J. Berliner and J. Reuben, Eds.), Vol. 1, p. 277. Plenum, New York, 1978.
43. Handreck, G. P., and Smith, T. D., *J. Chem. Soc. Faraday Trans.* **87**, 1025 (1991).
44. Tavernier, S. D., and Schoonheydt, R. A., *Zeolites* **11**, 155 (1991).
45. Walker, F. A., Sigel, H., and McCormick, D. B., *Inorg. Chem.* **11**, 2756 (1972).
46. Falk, K.-E., Ivanova, E., Roos, B., and Vanngard, T., *Inorg. Chem.* **9**, 556 (1970).
47. Adato, I., and Elezer, I., *J. Chem. Phys.* **54**, 1472 (1971).